Applied Acoustics 72 (2011) 78–88

Contents lists available at ScienceDirect

Applied Acoustics

journal homepage: www.elsevier.com/locate/apacoust

The use of Herschel–Quincke tubes to improve the efficiency of lined ducts

Benjamin Poirier *, Cédric Maury, Jean-Michel Ville

Laboratoire Roberval UMR UTC-CNRS No. 6253, Université de Technologie de Compiègne, BP 20529 F60205 Compiègne Cedex, France

ARTICLE INFO

Article history:
Received 17 June 2009
Received in revised form 11 August 2010
Accepted 26 September 2010
Available online 18 November 2010

Keywords:
Duct acoustics
Scattering matrix
Herschel–Quincke tubes
Liner
Muffler

ABSTRACT

The scattering matrix results of Herschel–Quincke (HQ) resonators installed in combination with an acoustic liner (HQ-Liners) are presented in this paper. This approach aims at controlling both tonal and broadband noise to improve the liner efficiency. It uses circumferential arrays of Herschel–Quincke tubes on a main duct in a serial association with a locally reacting liner of known impedance. Results for the scattering matrix of this system are deduced from an analytical model and compared with experimental and numerical data showing a good agreement. Analysis of the scattering matrix coefficients points out the modal conversion properties that depend on the number of HQ tubes along the circumference. Results of the transmission loss show that the choice of an optimal HQ configuration with respect to the liner properties can substantially improve the liner efficiency.

1. Introduction

The concept of Herschel–Quincke (HQ) waveguide resonators, introduced in the undulatory theory of light [1], has shown a great practical potential to reduce the inlet fan noise due to turbofan engines when combined with acoustic liners [2]. In order to adjust the HQ resonances to the blade passing frequencies, an adaptative HQ system was tested under the NASA/Honeywell Engine Validation Noise and Emissions Reductions Technologies (EVNERT) program for aft noise control on the Honeywell turbofan engine Tech977 [3,4]. Although the understanding of the physics of such an approach was not completely achieved, the experimental results showed that the performance of the production liner currently installed on the test engine was improved for some HQ-Liner configurations.

Despite a well-documented literature on the physics of Helmholtz and quarter-wave resonators, HQ-like systems have received much less attention. A one HQ-like attenuator with a right-angled bend has been theoretically and experimentally investigated by Fuller and Bies [5], showing large TL peaks at a series of discrete frequencies all below the first duct cut-on frequency. Acoustic wave propagation in a uniform 2D-lattice of interconnected tubes has been explored by Depollier et al. [6], showing pass and stop band transfer properties.

In 1994, a 1D model has been developed by Selamet et al. [7] to calculate the transmission loss (TL) of a one HQ tube system. Introducing an "effective" tube length to account for the curved-shaped tube–duct interface, a good correlation was found on the TL with respect to a finite-difference scheme and experiments performed in the plane wave region. The 1D model has been extended to a multiple HQ tube configuration [8] leading to more complicated TL properties, showing that, in general, the HQ tubes diameter influences the width of the TL bands and the HQ tubes length influences the system resonance frequencies. The 1D model has also been extended to account for the non-negligible effects of a low speed mean flow on the TL properties of a one and multiple HQ tube system [9,10].

A 3D bicylindrical model has been developed by the authors [11] for a multiple HQ tube duct system that correctly predicts the non-periodic variations of the reflexion and transmission coefficients of the system in the plane wave region without the need to introduce an effective tube length correction. The aim of this paper is to use the bicylindrical model to better understand how the TL properties of a multiple HQ tube configuration (with N_{HQ} tubes in the no-flow case) are modified when mounted in series with a liner.

Consequently this study shows how the liner transmission loss (TL) may be improved by mounting a HQ system with N_{HQ} tubes in a serial configuration with the liner. Consequently, the study is based upon the scattering matrix formalism which is applied to both HQ and liner sections independently and also to the HQ-Liner association. An analytical calculation of the HQ-Liner scattering matrix whose results are compared with the numerical and experimental ones for validating purposes, is expressed in terms of an algebraic product [12] of both HQ and liner analytical scattering matrices. The results are presented under higher order mode propagation and no mean flow conditions for a locally reactive liner.

* Corresponding author.
E-mail address: Benjamin.poirier1@free.fr (B. Poirier).

0003-682X/$ - see front matter © 2010 Elsevier Ltd. All rights reserved.
doi:10.1016/j.apacoust.2010.09.010

The paper is organised as follows. The theoretical basis of the propagation model and of the finite element method (FEM) which are developed to calculate the scattering matrix of the HQ section, the liner section and the HQ-Liner section are described in Section 2 before introducing in Section 3 the scattering matrix measurement procedure. In Section 4, the results of the scattering matrix coefficients performed with the analytical approach are compared with both numerical and experimental data. Then the efficiency of HQ-Liner association is discussed for several HQ configurations. Final remarks conclude the study in Section 5.

2. Theoretical basis

The analytical computation of the HQ-Liner serial association is based upon the scattering matrix formalism because it enables to physically understand the mechanisms involved to improve the efficiency in terms of acoustic power attenuation and transmission loss (TL) of this association.

2.1. Definition of the scattering matrix of a duct element

The fluid is assumed to be ideal and linear acoustic theory to be valid. The HQ-Liner duct is connected to two hard-walled cylindrical ducts at axial coordinates $z_L = z_2$ (L: left side) and $z_R = z_5$ (R: right side) as shown in Fig. 1. The acoustic pressure distribution in both cross sections is written in cylindrical coordinates (r, θ, z) as:

$$p(r,\theta,z,t) = \sum_{m=-\infty}^{+\infty} \sum_{n=0}^{\infty} P_{mn}(z)\Phi_{mn}(r,\theta)e^{-i\omega t}, \quad (1)$$

where $\Phi_{mn}(r,\theta) = J_m(\chi_{mn}/a)e^{-im\theta}$ are the rigid duct eigenfunctions; the integers m and n are respectively the angular and radial wave numbers; J_m is the Bessel function of the first kind of order m; χ_{mn}/a is the n^{th} root of the first derivative of J_m [13]. The total modal pressure coefficients $P_{mn}(z)$ in the cross sections located at axial coordinates z_L and z_R are given by the following relationship:

$$P_{mn}(z) = P^{+}_{mn}(z) + P^{-}_{mn}(z) \quad (2)$$

Pressure waves traveling along the positive and negative z directions in regions I and V are depicted by $P^{I\pm}_{mn}(z) = P^{\pm}_{mn}(0)e^{\pm ik_{mn}z}$ and $P^{V\pm}_{mn}(z) = P^{V\pm}_{mn}(0)e^{\pm ik_{mn}z}$, respectively. $k_{mn} = \sqrt{k^2 - (\chi_{mn}/a)^2}$ is the axial wavenumber of the (m,n) duct mode. The scattering matrix $[S]$ of a duct element located between the axial coordinates z_L and z_R relates the outgoing pressure wave vector $\{P^{\text{out}}\}_{2N} = \langle P^{I-}_{00}(z_L), \ldots, P^{I-}_{PQ}(z_L), P^{V+}_{00}(z_R), \ldots, P^{V+}_{PQ}(z_R)\rangle^{\mathrm{T}}_N$ to the incoming pressure wave vector $\{P^{\text{in}}\}_{2N} = \langle P^{I+}_{00}(z_L), \ldots, P^{I+}_{PQ}(z_L),\ P^{V-}_{00}(z_R), \ldots, P^{V-}_{PQ}(z_R)\rangle^{\mathrm{T}}_N$ (Fig. 1):

$$\{P^{\text{out}}\}_{2N} = [S]_{2N\times 2N} \times \{P^{\text{in}}\}_{2N} = \begin{bmatrix} [S^{11}]_{N\times N} & [S^{12}]_{N\times N} \\ [S^{21}]_{N\times N} & [S^{22}]_{N\times N} \end{bmatrix}_{2N\times 2N} \times \{P^{\text{in}}\}_{2N} \quad (3)$$

The vector $\{P^{in}\}_{2N}$ contains the modal incident pressures $P^{I+}_{mn}(z_L)$ coming in the element from the left side and the modal incident pressures $P^{V-}_{mn}(z_R)$ coming in the element from the right side. The vector $\{P^{\text{out}}\}_{2N}$ contains the modal reflected pressures $P^{I-}_{mn}(z_L)$ coming out the element from the left side and the modal pressures $P^{V+}_{mn}(z_R)$ transmitted on the right side of the element. N being the number of cut-on modes in both cross sections, P and Q are respectively the maximum angular and radial orders associated to the first N cut-on modes. The scattering matrix represents an intrinsic characterization of the duct element independently of the upstream and downstream acoustic conditions: It depends only on acoustic and geometric features of the test section. It is composed of $(2N)^2$ coefficients $S^{kl}_{mn,pq}$ with k, $l = 1,2$, $(\boldsymbol{m}, p) \in [0\ldots\boldsymbol{P}]$ and $(\boldsymbol{n}, \boldsymbol{q}) \in [0\ldots\boldsymbol{Q}]$. The properties per mode of the test element to reflect or to transmit waves coming from both sides are described by the scattering matrix $[S]$ coefficients. Indeed, each elementary matrix expresses a physical meaning:

- $\left[S^{11}_{mn,pq}\right]_{N\times N}$ the reflection of the wave coming in the element from the left side.
- $\left[S^{21}_{mn,pq}\right]_{N\times N}$ the transmission of the wave coming in the element from the left side.
- $\left[S^{22}_{mn,pq}\right]_{N\times N}$ the reflection of the wave coming in the element from the right side.
- $\left[S^{12}_{mn,pq}\right]_{N\times N}$ the transmission of the wave coming in the element from the right side.

2.2. Analytical calculation of the HQ-Liner scattering matrix

The HQ-Liner scattering matrix is deduced from the calculation of the scattering matrices of each element: the hard wall HQ-duct section and the liner section.

2.2.1. Analytical calculation of the HQ matrix

The analytical calculation of the HQ element is based upon a bicylindrical technique [11] that takes into account the real HQ tube–duct interface and the curved shape of the HQ tube.

2.2.1.1. Basic integral equation. Let consider in the no-flow condition the rigid-walled duct connected with N_{HQ} cylindrical HQ tubes

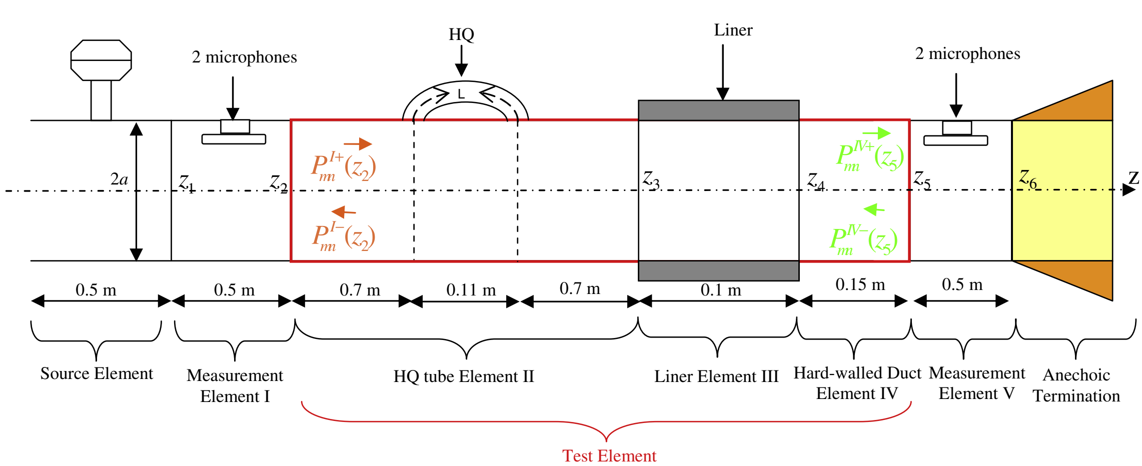

Fig. 1. Description of the HQ-Liner system.

located circumferentially around the duct (Figs. 1 and 2), sharing the same axial position between z_2 and z_3 and referred to as N_{HQ} HQ tubes as from here. The pressure $p(w)$ at any point with coordinates $w = (r,\theta,z)$ in the duct is written as the sum of the incident pressure $p^{\mathrm{inc}}(w)$ assumed to propagate towards the positive z direction in the straight duct without the HQ arrays and an integral over S_u, S_u being the elementary area of the main duct which communicates with an input or output of a HQ tube [14]:

$$p(w) = p^{\mathrm{inc}}(w) - i\omega\rho \sum_{u=1}^{2N_{HQ}} \bar{v}_u \int_{S_u} G(w,w')dS \tag{4}$$

where w' belongs to the surface S_u, G is the Green's function for the main duct, $\bar{v}_u$ is the averaged outward particle acoustic velocity normal to S_u, ρ is the fluid density and ω the angular frequency. The unknowns of the problem $\bar{v}_u$, $u = 1,\ldots,2N_{HQ}$, are assumed to be constant on all the surfaces. The Green's function is decomposed on the basis of the rigid wall cylindrical duct eigenmodes $\Phi_{mn}(r,\theta)$:

$$G(w|w') = \frac{i}{S} \sum_{m=-M_g}^{M_g} \sum_{n=0}^{N_g} \frac{\Phi_{mn}(r,\theta)\Phi_{mn}(a,\theta')}{2N_{mn}k_{mn}} e^{-ik_{mn}(z-z')} \tag{5}$$

where $S = \pi a^2$ is the duct cross section, M_g and N_g being the number of azimuthal and radial modes. The normalization factor N_{mn} is defined by:

$$N_{mn} = \begin{cases} J_m^2(\chi_{mn}) & \text{if } m = 0 \\ \frac{1}{2}\left[1 - \frac{m^2}{(\chi_{mn})^2}\right] & \text{if } m \neq 0 \end{cases} \tag{6}$$

In Eq. (4), the term $-i\omega\rho\bar{v}_u \int_{S_u} G(w,w')dS$ represents the pressure radiated at $w = (r,\theta,z)$ by an input or output HQ tube area located at $w_u = (a,\theta_u,z_u)$.

2.2.1.2. Tube modelling. As the HQ tube is assumed to be curved (Fig. 3) the reflection and transmission coefficient of this bend is performed based on a model developed by Bi et al. [12]. This multi-modal method is adapted to three-dimensional bends of circular cross section, in which the wave equation is not separable. In our case, only the plane wave coefficients of the curved tube HQ's scattering matrix, which is different from the plane wave coefficient of a straight HQ tube [12] are considered. The sound field inside a tube is expressed in terms of positive and negative travelling plane waves. The acoustic pressure and particle velocity at the ends of the tube can be expressed in the following matrix form:

$$\begin{Bmatrix} \bar{p}^t_{ui} \\ \bar{p}^t_{uo} \end{Bmatrix}_{2\times1} = \begin{bmatrix} Z^{tl}_{ii} & Z^{tl}_{io} \\ Z^{tl}_{oi} & Z^{tl}_{oo} \end{bmatrix}_{2\times2} \begin{Bmatrix} \bar{v}^t_{ui} \\ \bar{v}^t_{uo} \end{Bmatrix}_{2\times1} \tag{7}$$

where Z^{tl}_{ii}, Z^{tl}_{io}, Z^{tl}_{oi}, Z^{tl}_{oo} are the terms of the impedance matrix, L is the length of the tube, the indices i and o refer respectively to the entry and the exit of the tube. After assembling the matrices for each HQ tube, the total matrix relating the pressure and the velocity at the entry and exit of each tube is deduced:

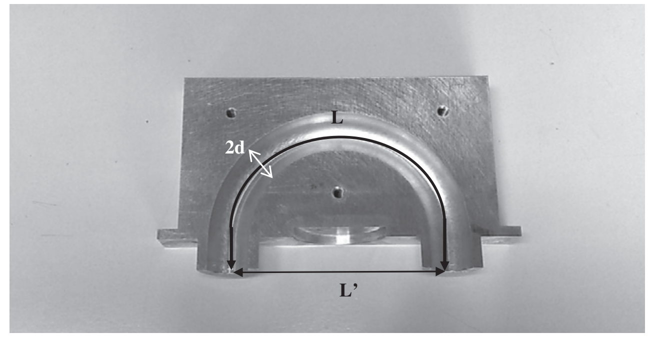

Fig. 3. Cross sectional view of HQ tube.

$$\{\bar{p}^t_u\}_{2N_{HQ}} = [Z_{HQ}]_{2N_{HQ}\times 2N_{HQ}} \{\bar{v}^t_u\}_{2N_{HQ}} \tag{8}$$

2.2.1.3. Tube duct coupling. The model for the coupled tube–duct system is obtained by matching at the tube–duct interface the averaged pressures, i.e $\bar{p}_{ui} = \bar{p}^t_{ui}$ and the averaged velocities, i.e $\bar{v}_{ui} = \bar{v}^t_{ui}$; The velocity at the tube–duct interfaces is obtained after substituting (4) and (8) within the continuity conditions. It is expressed as a function of the impedance matrix of the tube–duct system and the incident pressures $\bar{p}_u$ averaged on the interfaces:

$$\{\bar{v}^t_u\}_{2N_{HQ}} = [Z_{HQ} - Z_{rs}]^{-1}_{2N_{HQ}\times 2N_{HQ}} \{\bar{p}_u\}_{2N_{HQ}} \tag{9}$$

2.2.1.4. Analytical expression of the HQ scattering matrix. The modal incident pressure can be expressed as a vector:

$$\begin{aligned} \{\bar{p}_u\}_{2N_{HQ}} &= \{\bar{p}^{\mathrm{inc}}(w_1), \bar{p}^{\mathrm{inc}}(w_2), \ldots, \bar{p}^{\mathrm{inc}}(w_{2N_{HQ}})\}^{\mathrm{T}} \\ &= \left\{\boldsymbol{\beta}^+_1 \boldsymbol{P}^{I+}, \boldsymbol{\beta}^+_2 \boldsymbol{P}^{I+} \ldots, \boldsymbol{\beta}^+_{2N_{HQ}} \boldsymbol{P}^{I+}\right\}^{\mathrm{T}} \end{aligned} \tag{10}$$

where the modal incident vector $\boldsymbol{P}^{I+}$ is defined as $\boldsymbol{P}^{I+} = \left\{P^{I+}_{00} \quad \cdots \quad P^{I+}_{PQ}\right\}^{\mathrm{T}}$ and $\boldsymbol{\beta}^+_u = \{\beta^+_{u,1} \quad \cdots \quad \beta^+_{u,PQ}\}$. The computation of $\beta^+_{u,mn} = J_{mn}(\chi_{mn}) \frac{1}{S_u} \int_{S_u} e^{-im\theta} e^{-ik_{mn}z} dS$ is detailed in [11]. From Eqs. (9) and (10), the vector of the total modal transmitted amplitudes expressed as a function of the vector of the modal incident pressures is deduced:

$$\{p^+_{\mathrm{tot}}\}_{N\times1} = [S^{21}]_{N\times N} \boldsymbol{P}^{I+}_{N\times1} \tag{11}$$

with

$$[S^{21}]_{N\times N} = \begin{bmatrix} \alpha^+_{1,00} & \cdots & \alpha^+_{2N_{HQ},00} \\ \alpha^+_{1,10} & \cdots & \alpha^+_{2N_{HQ},10} \\ & \vdots & \\ \alpha^+_{1,PQ} & \cdots & \alpha^+_{2N_{HQ},PQ} \end{bmatrix} [Z_{HQ} - Z_{rs}]^{-1}_{2N_{HQ}\times 2N_{HQ}} [\beta^+]_{2N_{HQ}\times N} + [I]_{N\times N}$$

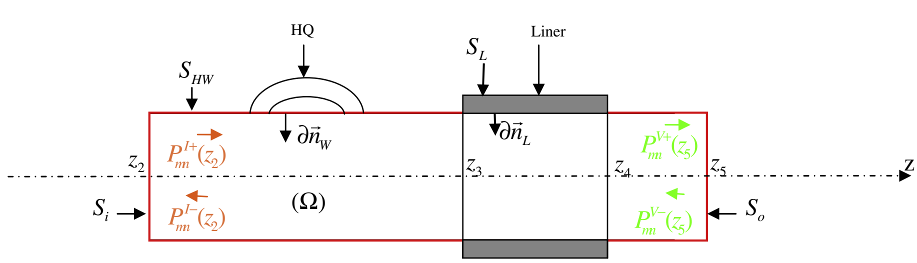

Fig. 2. Schema of the numerical formulation.

where $S^{21}]_{N\times N}$ is the transmission matrix related to the wave coming into the test element from the left side and $\alpha^{\pm}$ the modal transfer matrix for N_{HQ} tubes. To calculate the total reflected modal pressures, pressures radiating toward the negative z-direction by all sources are added:

$$p^{-}_{tot,mn} = \sum_{u=1}^{2N_{HQ}} \alpha^{-}_{u,mn}[Y][\beta^{+}]\boldsymbol{P}^{I+}_{N\times 1} \tag{12}$$

The vector of the total modal reflected amplitudes can then be expressed as a function of the modal incident pressure vector:

$$\{p^{-}_{\text{tot}}\}_{N\times 1} = [S^{11}]_{N\times N}\boldsymbol{P}^{I+}_{N\times 1} \tag{13}$$

where $[S^{11}]_{N\times N}$ is the reflection matrix of the wave coming in the element from the left side. Because of the symmetry of the HQ element, $[S^{1,1}]_{N\times N} = [S^{2,2}]_{N\times N}$ and $[S^{2,1}]_{N\times N} = [S^{1,2}]_{N\times N}$ and the expression of the matrix $[S]^{HQ}_{2N\times 2N}$ is deduced from Eq. (3).

2.2.2. Analytical calculation of the liner scattering matrix

The Multi-Modal Propagation Method (MMPM) developed by Bi et al. [12] has been used to estimate the liner scattering matrix $[S]^{\text{Liner}}_{2N\times 2N}$. The liner impedance of the segment between z_3 and z_4 (Fig. 2) is assumed to be locally reacting type and constant on all the duct area (Appendix A). The principle of the method is to expand the pressure and axial velocity into double infinite series using the rigid duct modal basis $\{\Phi_{mn}\}$, and then to follow the projection coefficients variations along the duct axis.

2.2.3. Analytical calculation of the HQ-Liner scattering matrix

The scattering matrices obtained for individual segments HQ, liner and rigid duct are then combined to construct the HQ-Liner scattering matrix $[S]^{tot}_{2N\times 2N}$. The combined element made by the juxtaposition of the three elements HQ, liner and rigid duct, may be directly written by performing a simple composition law [12] detailed in Appendix B. In view of Fig. 1, the scattering matrix $[S]^{tot}_{2N\times 2N}$ is then obtained as follows:

- The HQ scattering matrix $[S]^{HQ}_{2N\times 2N}$ of Element II located between z_2 and z_3.
- The liner scattering matrix $[S]^{Liner}_{2N\times 2N}$ of Element III located between z_3 and z_4.
- The rigid scattering matrix $[S]^{Rigid}_{2N\times 2N}$ of Element IV located between z_4 and z_5.

2.3. Numerical approach

To validate the analytical modelling of the HQ-Liner scattering matrix a 3D-finite element method (FEM) was conducted assuming that the acoustic pressure in the duct is solution of the following system (Fig. 2):

$$\begin{cases} (\Delta + k^2)p = 0 \ (\Omega) \\ \frac{\partial p}{\partial n_W} = 0 \ (S_{HW}) \\ Z\frac{\partial p}{\partial n_L} = i\omega\rho p \ (S_L) \end{cases} \tag{15}$$

where ∂n_W is the inward derivative normal to the wall duct surface S_{HW}, S_L is the boundary of the lined wall duct with normal vector n_L. The liner is assumed to be locally reacting with normalized acoustic impedance Z. The Helmholtz's equation is integrated over a finite internal volume Ω limited by the inlet section S_i and the outlet section S_o and by the hard walls of the duct and the HQ tubes. At the inlet section S_i, a constant total pressure is imposed at z_2 to produce an incident plane wave. At the outlet section S_o located at z_5 a Perfectly Matching Layer (PML) [16] condition is assumed to simulate the anechoic termination. This boundary-value problem is solved with a standard finite element method. The Helmholtz equation is written following the weak variational formulation

$$-\int_{\Omega}(\nabla q \cdot \nabla p)d\Omega + k^2\int_{\Omega} qp\, d\Omega + \int_{S_L} q\frac{\partial p}{\partial n}dS_L = 0, \tag{16}$$

with q a test function. The finite element method is implemented using isoparametric tetrahedral elements with quadratic interpolation functions. To ensure the convergence, a mesh (19805 nodes) satisfying a criterion of 10 nodes per wavelength near the singularities was chosen (Fig. 4). The origin of the z axis is taken at the reference phase in the inlet section S_i (Fig. 2). A technique to separate incident and reflected waves, similar to this used in the experimental procedure, is achieved based on the acoustic pressure fields calculated in each of the two pairs of cross section areas. Six hundred and twenty-five-points have been chosen to ensure the accuracy of modal decomposition in the cross sections. For computing the numerical scattering matrix the experimental procedure described in Section 3.2 is used.

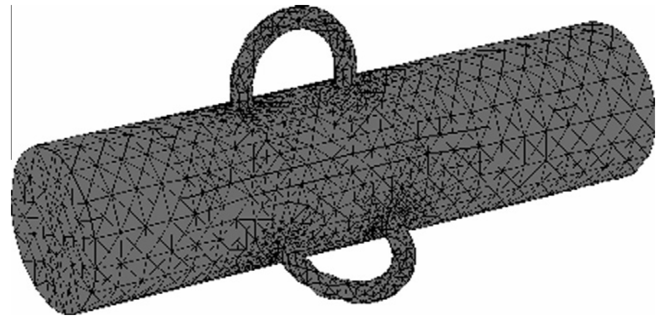

Fig. 4. Meshing of the 3HQ configuration.

3. Experimental set-up

Measurement of the 1HQ-Liner scattering matrix has been carried out in the no-flow case with the UTC duct acoustic facility built under a grant with E.E.C. during the Ducat program (Fig. 5). The experimental procedure was developed with this facility during a previous work and already tested on duct discontinuities under higher-order mode propagation conditions [13].

3.1. Description of HQ-Liner association tested

The duct element, the scattering matrix of which is studied, is located between z_2 and z_5 (Fig. 1) 0.5 m apart and is composed of

Fig. 5. The UTC duct acoustic facility.

three parts: 0.25 m long HQ section, 0.1 m long lined wall section and 0.15 m hard wall duct. The liner made of a perforated plane, a honeycomb and backed by a rigid plate is assumed to be locally reacting (Fig. 6). The normalized acoustic impedance of the liner is calculated with a semi-empirical modeling [15]. Results plotted versus ka in Appendix A point out a liner resonance frequency at $ka = 2.18$ given a honeycomb thickness of 0.02 m (a is the internal duct radius equal to 0.075 m and k the acoustic wavenumber), e.g. below $ka = 3.8$ under low-order multi-modal propagation conditions. As shown in Fig. 6, a 0.001 m hole diameter has been chosen as a compromise between high absorption at the liner resonance and bandwidth. The study is conducted within the non-dimensional frequency band ka [0–3.8] leading up to $N = 5$ cut-on modes ((0,0); (±1,0); (±2,0)) with the (±1,0) and (±2,0) modes respectively cut-on at ka = 1.841 and 3.054.

All the HQ tubes installed during the experiments are identical with a radius $d = 0.02$ m, a length $C = 0.205$ m and the distance between the input and output interfaces $L' = 0.11$ m (Fig. 3). The main duct diameter of 0.15 m is imposed by the acoustic duct facility. The geometrical parameters of each HQ tube have been chosen in broad agreement with those implemented for aft fan noise control [3], although about 40 of them were used at two axial positions at the turbofan inlet. Issues on the sound power reduction predicted on a real turbofan are far beyond the scope of this paper and would require a more practical modelling of the HQ tube–duct system accounting for mean flow effects, especially at the wire-mesh HQ tube openings and under high pressure levels. More specifically, in view of Refs. [8,11], the HQ tubes diameter has been chosen small enough to ensure well localized TL peaks and large enough for the HQ tubes still to be efficient. Indeed, parametric studies [11] have shown that increasing the tubes cross sectional area increases the amplitude and bandwidth of the TL peaks and shifts down the frequency location of the TL peaks due to a larger effective tube length at the saddle-shaped interface. Increasing the number of identical HQ tubes with equivalent total branch cross sectional area increases the TL peak amplitudes and shifts up the TL peaks location, as it will be observed in Section 4.2.1 on the reflection coefficient. It also introduces circumferential modal scattering as it will be seen and thus increases the broadband sound power reduction. This last feature is broken down if one considers HQ tubes with different diameters as the circumferential spacing is then not uniform so that scattering onto high order circumferential modes does not occur and the broadband TL decreases. Finally, it has been observed that increasing the centerline tube length L shifts down the HQ resonance frequencies and lowers the TL peak amplitudes. A value $L = 0.205$ m has been chosen in order to have a HQ resonance frequency between each duct cut-on frequency below ka = 3.8, i.e. for each modal propagation condition. The value of L', the distance between the tube ends, depends on L if one assumes a semi-circular centerline.

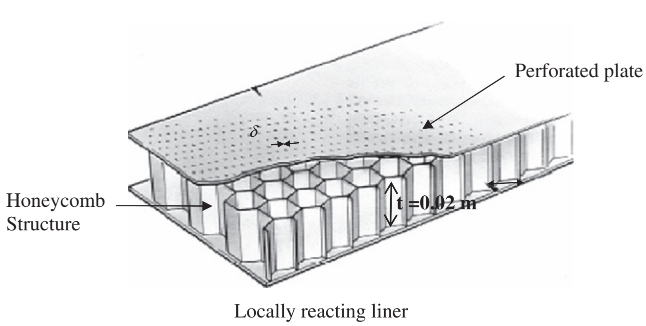

Fig. 6. Description of the liner.

3.2. Experimental flow chart

The experimental procedure with the source located on the left side and an anechoic termination is described by the flow chart in Fig. 7. The study is conducted within the non-dimensional frequency band ka [0–3.8] leading up to $N = 5$ cut-on modes ((0,0); (±1,0); (±2,0)). The experiment provides at two cross sections located at z_L and z_R the modal distributions of the incoming and outgoing pressure waves. This is achieved by a modal decomposition technique [17,18] of the total complex pressures $p(r,\theta)$measured at two pairs of cross sections located on each side of the test element followed by a separation technique into incident and reflected waves. The HQ-Liner test section is not symmetrical and requires both side excitations to compute the scattering matrix [S]. Because of a hardware limitation to move the source section on the right side, the experiment is conducted in two steps (Fig. 8) reversing the duct under test.

The procedure of each step is repeated for $L \times N$ ($L \geqslant 1$) source configurations [17] chosen to ensure the generation of linearly independent input modal vectors $\left\{P^{I+}_{mn}(z_L)\right\}, \left\{P^{V+}_{mn}(z_R)\right\}, \left\{P^{I-}_{mn}(z_L)\right\}$ and $\left\{P^{V-}_{mn}(z_R)\right\}$ to fill the matrices $[P^{\text{in}}]_{2N\times LN}$ and $[P^{\text{out}}]_{2N\times LN}$. Finally all the coefficients of the matrix $[S^{11}]_{N\times N}$ and $[S^{21}]_{N\times N}$ are determined as described in Fig. 7. The measurement of the $[S^{22}]_{N\times N}$ and $[S^{12}]_{N\times N}$ matrices is performed in the second step with the same procedure but reversing the duct element. As only cut-on modes are taken into account, the rank of [S] depends upon the frequency.

Indeed, the influence of the cut-off modes is neglected assuming that the measurement sections, z_L and z_R, are far enough from the discontinuities located at the hard wall-liner interface and at the HQ opened sections. This justifies the use of the hard-walled duct element IV shown in Fig. 1.

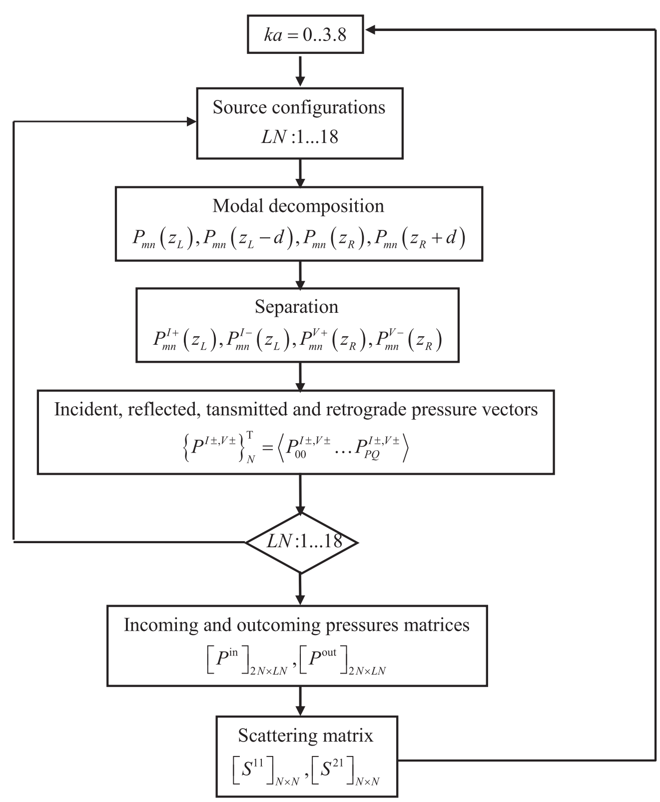

Fig. 7. Flow-chart for scattering matrix measurement.

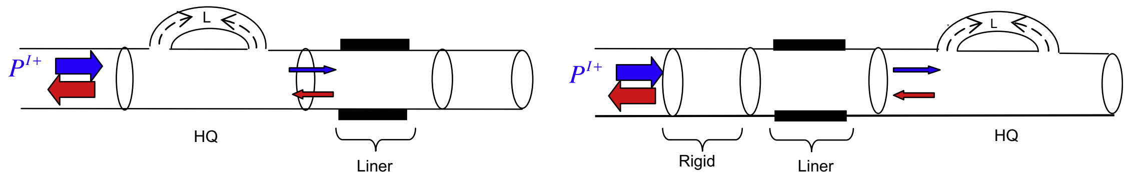

Fig. 8. The two experimental serial associations.

4. Results

In this section the HQ-Liner duct element scattering matrix results performed with the analytical modeling are presented for validation purpose. Then, the relationship between the modal conversion phenomenon and the number of HQ tubes is established in order to explain how the liner TL performance is improved by the HQ section.

4.1. Validation of the analytical modeling

To validate the analytical model, the results of some typical scattering matrix coefficients are compared with FEM and experimental data for a 1 HQ tube configuration in series with the liner section. The analytical moduli of the HQ-Liner duct scattering matrix coefficients for modes (0,0), (1,0) and (2,0) are calculated using the bicylindrical modelling [6] and compared respectively in Figs. 9–11 with the experimental and numerical FEM results for left side incident pressure waves up to $ka = 4$, showing a good agreement over all the coefficients. The reflection coefficient $\left|S^{1,1}_{00,00}\right|$ and the transmission coefficient $\left|S^{2,1}_{00,00}\right|$ for the plane wave are plotted versus ka in Fig. 9. Below $ka = 1.1$, the experimental values of $\left|S^{1,1}_{00,00}\right|$ and $\left|S^{2,1}_{00,00}\right|$ are respectively close to 0 and 1 except for very low frequency because of a high uncertainty during the separation procedure [17]. When frequency is getting closer to $ka = 1.1$ which corresponds to the first HQ-duct resonance, the transmission coefficient decreases from 1 to 0.6, thus pointing out a tonal reduction confirmed by the FEM and the bicylindrical model. The HQ frequencies are predicted within a total error of 6% compared with the FEM results although it somewhat under predicts the maximum amplitudes with for instance, a decrease of the reflection coefficient from 1 to 0.4 at $ka = 1.1$. The accuracy of the analytical technique could be improved when fully accounting for the local variations of the acoustic velocity along the saddle-shaped tube–duct interface, instead of only assuming a volumetric contribution (see Eq. (4)). This causes the differences observed in Fig. 9 with respect to the baseline FEM results. For $1.1 \leqslant ka \leqslant 2.18$, the transmission coefficient in Fig. 9 decreases to 0 which corresponds to the broadband attenuation of the liner. The numerical results show a local discrepancy compared with the measured ones, due to the difficulty of meshing the saddle-shaped tube–duct interface in order to correctly account for local variations of the evanescent components. A uniform grid having a density high enough so that the local errors estimated in these difficult regions are acceptable could be performed. But this approach is computationally extremely costly. In Fig. 9, a tonal attenuation is observed at $ka = 3.3$ with a fall on the transmission coefficient which decreases locally from 1 to 0.6 due to the third HQ resonance. The differences observed around the liner resonance come from the impedance model (A.1) which is limited at high frequencies [15].

The modulus of the scattering matrix coefficients of the HQ-Liner system are plotted in Figs. 10 and 11 for respectively the modes (1,0) and (2,0). The analytical model predicts an increase with ka of both transmission coefficients $\left|S^{2,1}_{10,10}\right|$ and $\left|S^{2,1}_{20,20}\right|$ above their cut-on frequencies in good agreement with the HQ results deduced from the FEM method and the experiment. The Fig. 10 shows that, apart from the frequency band $1.5 \leqslant ka \leqslant 3.2$, the treatment is less efficient outside this bandwidth. It also noted that around the liner resonance $ka = 2.18$, which is very close to the second HQ resonance at $ka = 2.2$, the HQ effect is "hidden" in transmission whereas it appears with a drop in reflection followed by an increase in amplitude to reach a value close to 0.7. After $ka = 3.1$ in Fig. 11, the modulus of the transmission coefficient of mode (2,0) should rapidly increase as a function of frequency from 0 to 1. However, a slowly increasing transmission coefficient is observed. This trend was already observed by Sitel [13] and by Taktak [19] who attributed this slow increase to the non-respect of zero velocity at the duct wall just above the (2,0) mode cut-on frequency. This effect does not appear in Fig. 10 for the transmission of the mode (1,0) because it is hidden by the liner's dissipation in

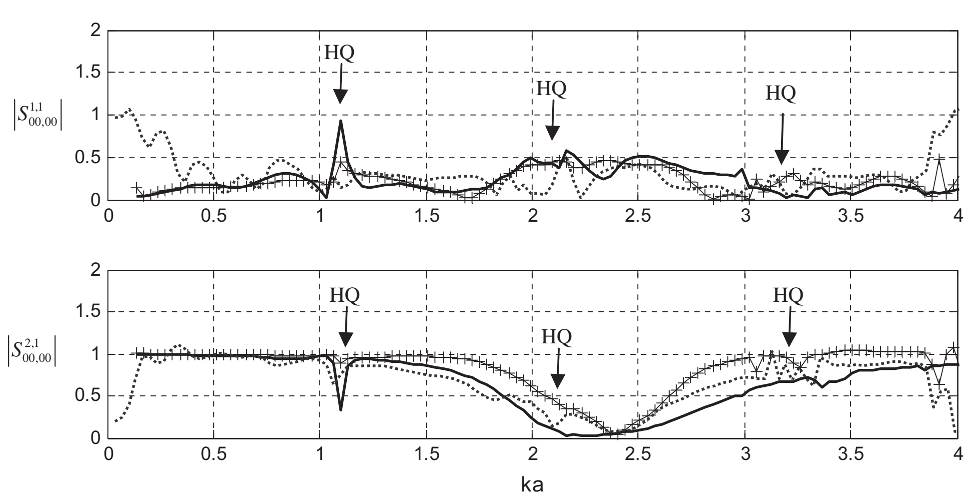

Fig. 9. The reflection $S^{1,1}_{00,00}$ and transmission $S^{2,1}_{00,00}$ scattering matrix coefficients for mode (0,0) and a 1HQ-Liner configuration versus ka: Bicylindrical FEM Experiment.

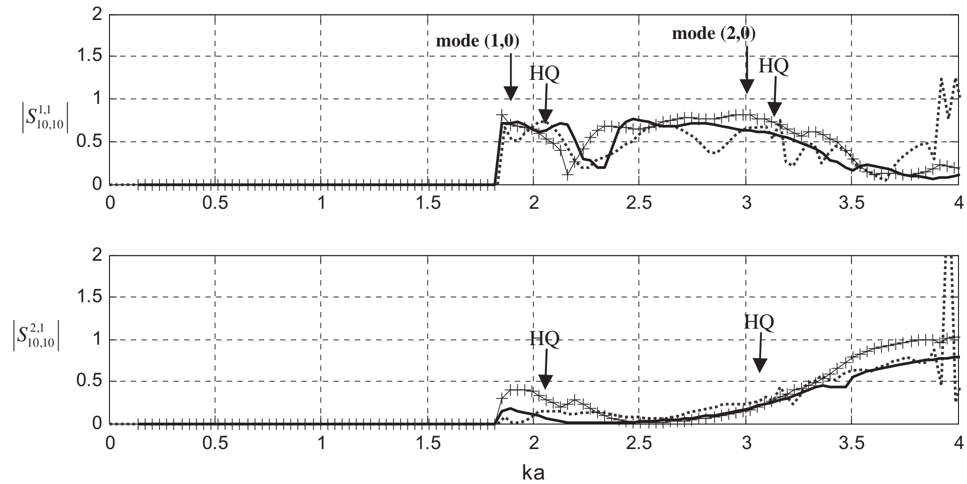

Fig. 10. Scattering coefficient of reflection $S^{1,1}_{10,10}$ and transmission $S^{2,1}_{10,10}$ of the mode (1,0) for 1HQ-Liner configuration; Bicylindrical FEM Experiment.

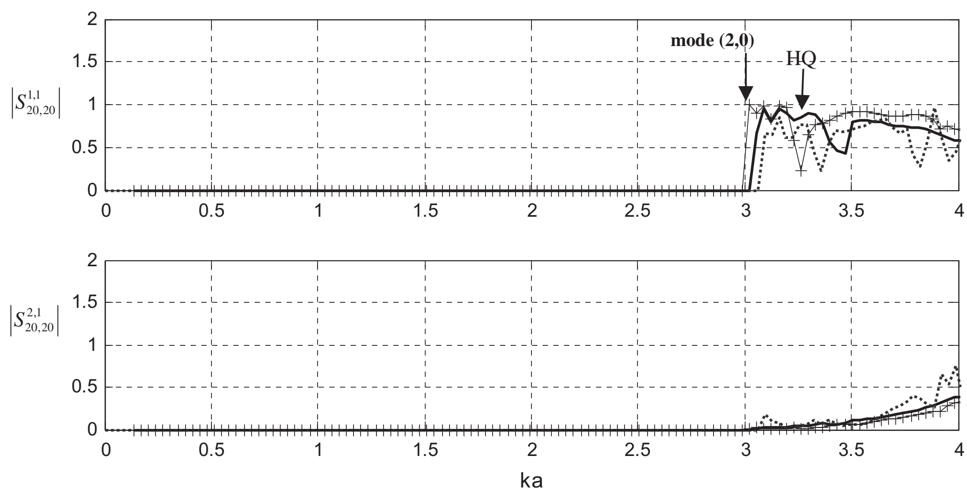

Fig. 11. Scattering coefficient of reflection $S^{1,1}_{20,20}$ and transmission $S^{2,1}_{20,20}$ of the mode (2,0) for 1HQ-Liner configuration; Bicylindrical FEM Experiment.

the frequency band $1.5 \leqslant ka \leqslant 3.2$. The modulus of the scattering coefficients in transmission and reflection of the mode (2,0) in Fig. 11 shows that even at high frequencies, the agreement between theory and experiment is good. At the frequency $ka = 3.3$, the third HQ resonance frequency, the experimental and numerical results disagree because of the non-volumetric contribution of evanescent modes at the saddle-shaped interface. The differences observed between analytical results and FEM results can be explained by the assumption of considering the normal acoustic velocity at the interface as constant for the analytical model which is actually not the case [11]. An overall agreement is observed in Figs. 9–11 between the FEM results and the measured scattering coefficients. However, discrepancies are noted, especially near the first duct cut-on frequencies around $ka = 1.84$, 3.05 and 3.83. These are due to inaccurate measurement of the phase differences between the microphone signals which become very small near cut-off and lead to a decrease of the signal-to-noise ratio. Increasing the number of sources and a more accurate phase calibration of the microphones would improve the accuracy of the measurements. Also, the local differences observed in Figs. 9 and 10 above the first duct cut-on frequency are certainly due to minor geometrical features in the experimental set-up, such as added dissipation/transmission at the tube–duct junction, and non-perfect duct wall rigid condition, that might modify the amplitude of the coefficients just above the first duct cut-on frequency where the first transverse mode strongly excite the duct wall. Finally, the accuracy of the FEM results might be improved if losses due to viscous propagation effects, which are influent close to the duct cut-on frequencies and to the HQ-duct resonance frequencies, are accounted for, especially at the junctions and within the curved tubes. This would explain why the FEM-based scattering coefficients are essentially above the measured ones when differences are observed.

4.2. Noise control by the HQ section to improve the liner transmission loss

The HQ-Liner scattering matrix transmission loss (TL) is deduced as detailed in Appendix C from the scattering matrix for the following plane wave vector incoming the duct element from the left side:

$$\{P^{\text{in}}\} = \langle 1 \quad 0 \quad 0 \quad 0 \quad 0 \quad 0 \quad 0 \quad 0 \quad 0 \quad 0 \rangle^T \tag{17}$$

The analysis of the TL results is based on the modal conversion property of the HQ section which is pointed out through the study of the HQ section scattering matrix coefficient varying N_{HQ} the number of HQ tubes.

4.2.1. The HQ modal conversion mechanism

The number of tubes N_{HQ} is a determinant criterion governing the scattering process as shown in Fig. 12 where the HQ section matrix coefficients $\left|S^{1,1}_{00,00}\right|$ predicted by the analytical modeling with N_{HQ} = 1, 2, 3 are plotted versus ka. Indeed, an increase in N_{HQ} leads to an increase in phase cancellation at the HQ frequencies which in addition shift with N_{HQ} around ka = 1.1, ka = 2.2 and ka = 3.3. At ka = 2.2, the reflection coefficient increases from 0 to 0.3 for 1 tube and from 0 to 1 for 2 and 3 tubes. The recombination of scattered energy and the phase cancellation into higher modes contributes to the noise reduction as well as N_{HQ} increases. Fig. 13 shows that the propagation and the redistribution of energy into other circumferential modes is controlled by increasing N_{HQ}. Fig. 13a–c presents the scattering coefficients from the mode (0,0) towards respectively the modes (1,0), (2,0) and (3,0) when varying N_{HQ}. It shows that, whatever the number of tubes considered, the frequencies at which a maximum of modal conversion is observed coincides with the HQ resonances, i.e. the frequencies at which a minimum of transmission associated with a maximum of reflection is observed. Indeed, Fig. 13a points out that for one tube, the scattering matrix coefficient from the mode (0,0) to the mode (1,0) presents a maximum scattering effect with respect to the same frequencies as those observed in Fig. 9 for ka = 1.1 and ka = 3.3, corresponding to the first and third HQ resonances. Similarly, Fig. 13b shows that the conversion factor for one tube presents a maximum at ka = 3.3 as observed in Fig. 10.

Hence, for a given incident mode with a circumferential order m_{inc}, some of the modes present in the duct with the HQ tubes system can have circumferential order different than the disturbance circumferential order m_{inc}. This effect can be predicted. Fig. 13a and b shows that for a 1HQ tube configuration, the mode (0,0) is only scattered into the mode (1,0) at the frequencies ka = 1.1 and ka = 3.45 and into the mode (2,0) at the frequency ka = 3 while for the two tubes configuration, there is only scattering effect over the mode (2,0) (Fig. 13b) because the reflection coefficient is null over all the frequency band (Fig. 13a). For the three tubes configuration, the mode (0,0) is scattered just into the mode (3,0) (Fig. 13c). So the circumferential order m_{HQ} obtained by scattering redistribution is related with the number of tubes and the incident circumferential order m_{inc} through the rule already established by Hallez [14]:

$$m_{HQ} = m_{inc} + k_{HQ} N_{HQ} \tag{18}$$

where k_{HQ} = 0, ± 1, ± 2, ± 3. . ..

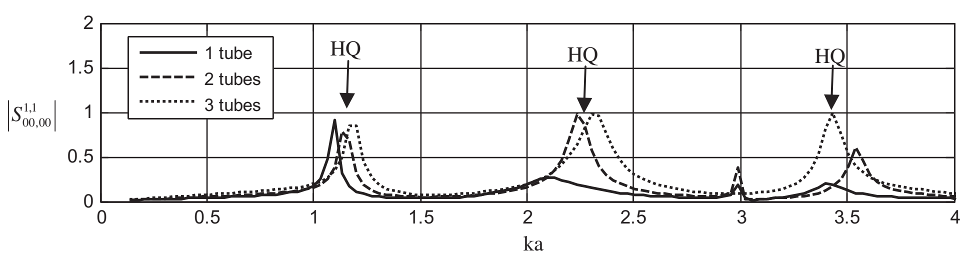

Fig. 12. The reflection scattering matrix coefficient $S^{1,1}_{00,00}$ of the HQ element versus ka for N_{HQ} = 1, 2, 3.

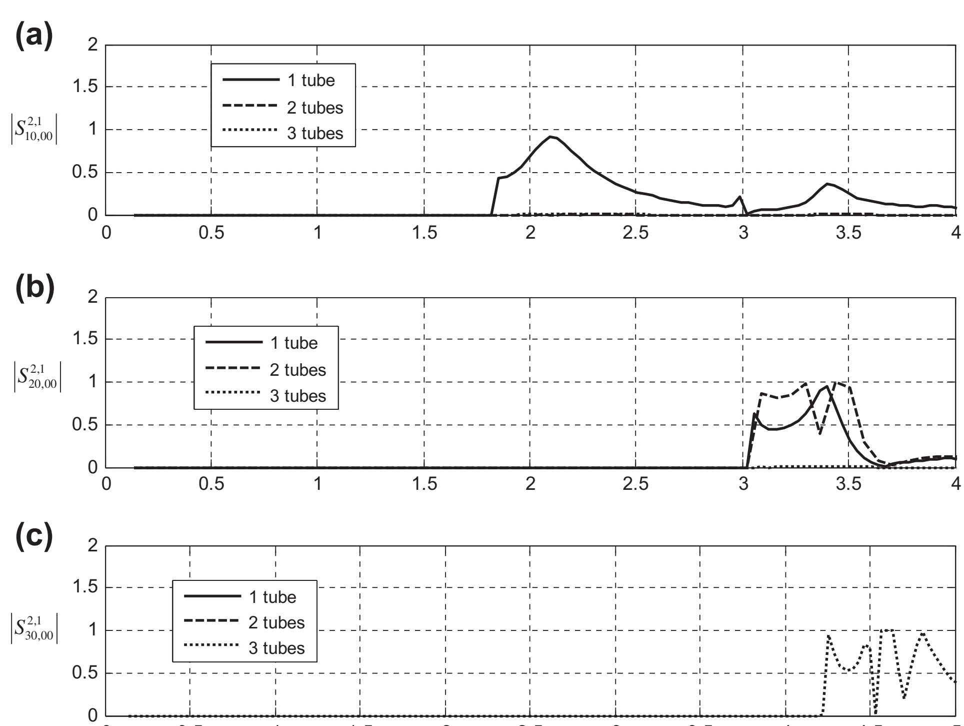

Fig. 13. The (0,0) transmission conversion scattering coefficients of the HQ element versus ka for N_{HQ} = 1, 2, 3: (a) towards (1,0); (b) towards (2,0) and (c) towards (3,0).

4.2.2. HQ effect on liner efficiency

The TL representation allows estimating the performance of the silencer because it takes into account both reactive and dissipative properties. The relationship between the HQ modal conversion property and the efficiency of the HQ-Liner muffler is pointed out by comparing in Fig. 14 the TL of a 1HQ-Liner configuration and of a 3HQ-Liner configuration. As shown when comparing Fig. 14 to Figs. 12 and 13, local TL peaks appear at the HQ-duct resonance frequencies which generate a large reflection and little transmission of the incident mode, e.g. at the HQ resonances below the first duct cut-on frequencies at which the incident mode is scattered into higher-order circumferential modes, according to Eq. (18), which are transmitted and eventually dissipated by the liner. The influence is evident around the second and third HQ resonance frequencies where the modal conversion between azimuthal modes with $N_{HQ} = 3$ was avoided (Figs. 12 and 13) increasing the plane wave reflection coefficient. The 3HQ-Liner TL shows an increase of 4 dB at the first HQ frequency and 18 dB compared to 1HQ-Liner case around the liner resonance frequency at $ka = 2.18$. At the third HQ resonance frequency the TL is increased by 27 dB when it is not even present for the 1HQ-Liner configuration. To assess the influence of the serial association, the TL of the 1HQ-Liner configuration is compared with the TL of the Liner and of the 3HQ-Liner configurations around the three HQ resonance frequencies (Tables 1 and 2). First in Table 1, results are presented around $ka = 2.2$ where the second HQ frequency is close to the liner resonance frequency. It points out an increase of 12.8 dB in the TL when the liner is combined with the 3HQ section instead of the 1HQ section.

$$\mathrm{TL(3HQ + Liner) = TL(3HQ) + TL(Liner) + 13\ dB} \tag{19}$$

$$\mathrm{TL(1HQ + Liner) = TL(1HQ) + TL}(Liner) + 0.7\ \mathrm{dB} \tag{20}$$

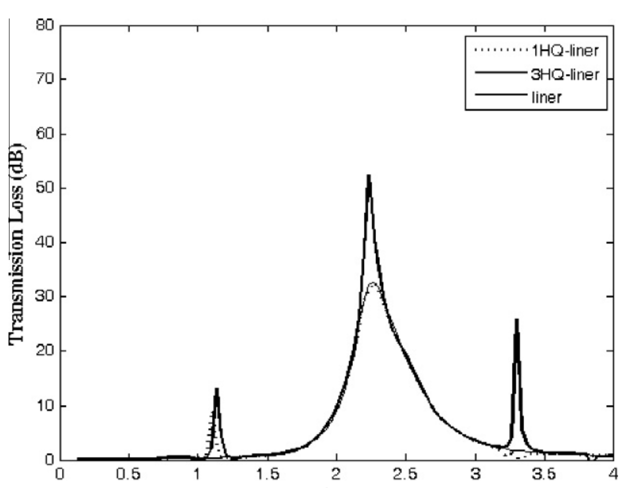

Fig. 14. The HQ-Liner and Liner alone analytical transmission loss versus ka for a plane wave incident vector and $N_{HQ} = 1,3$.

Table 1
Comparison for $N_{HQ} = 1, 3$ of the HQ-Liner TL with the TL of each element around $ka = 2.2$.

N_{HQ}	1	3
TL HQ	0.6	4.2
TL liner	29	29
TL HQ-Liner	30.3	46

Table 2
HQ influence on liner efficiency (in dB) for 3 tubes at HQ frequencies $ka = 1.1$ and $ka = 3.3$.

	$ka = 1.1$	$ka = 3.3$
TL 3HQ	5.5	20
TL liner	0.5	2.5
TL 3HQ-Liner	6	22.5

To explain this result, in Fig. 15 the attenuation of the liner alone which displays only the acoustic power dissipated is compared with the attenuation of the HQ-Liner configurations for $N_{HQ} = 1, 2, 3$ and a plane wave incident vector in front of the HQ element. The Vertical axis in Fig. 15 is indeed the attenuation, and not the TL. The attenuation has been defined in Appendix C, Eqs. (C.1) and (C.9) as the ratio between the incoming and outgoing acoustic powers. It characterizes only the intrinsic dissipation of the test duct whereas the TL characterizes both the reactive and dissipative properties of the test duct.

As expected the attenuation is close to zero at the HQ resonance frequencies where $\left|S^{1,1}_{00,00}\right|$ (Fig. 9) is close to 1. The dissipation of the HQ-Liner association (defined in Appendix C Eqs. (C.1) and (C.9)) is amplified by respectively 22 dB and 13 dB at frequencies just before and after the second HQ resonance frequency where the reflection coefficient $\left|S^{1,1}_{00,00}\right|$ increases with N_{HQ} without reaching 1 then leaving the wave being reflected and dissipated by the liner located downstream the HQ. Thus a self maintained state of stationary waves appears with multiple reflections between the HQ and the liner increasing the attenuation. Results presented in Table 2 show that around the first and third HQ frequencies where the liner shows less efficiency than around the second HQ resonance, but still an attenuation of 3 dB at $ka = 3.3$, the TL enhancement due to the serial association with 3HQ tubes is only the addition of the TLs of each element. However, one observes in Fig. 15 that the attenuation drops near these frequencies, and also near the second HQ resonance frequency with a pass-window opened around $ka = 2.2$, since what is reflected upstream at the HQ tube–duct resonance frequencies is not dissipated within the liner.

Fig. 16 presents a comparison between the measured attenuation and the one calculated using the bicylindrical theory for the 1HQ-Liner configuration. An overall agreement is found despite dips in the attenuation, which are predicted at $ka = 2.2$ and $ka = 3.4$, slightly above those measured at $ka = 2.1$ and $ka = 3.3$.

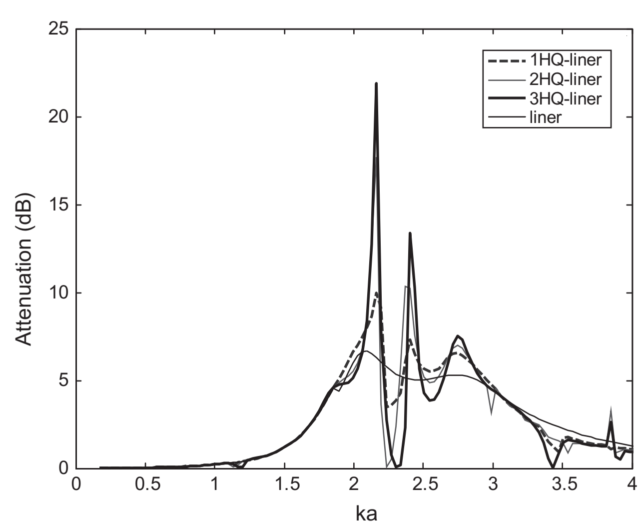

Fig. 15. The HQ-Liner acoustic power attenuation for a plane wave incident vector versus ka for $N_{HQ} = 1, 2, 3$.

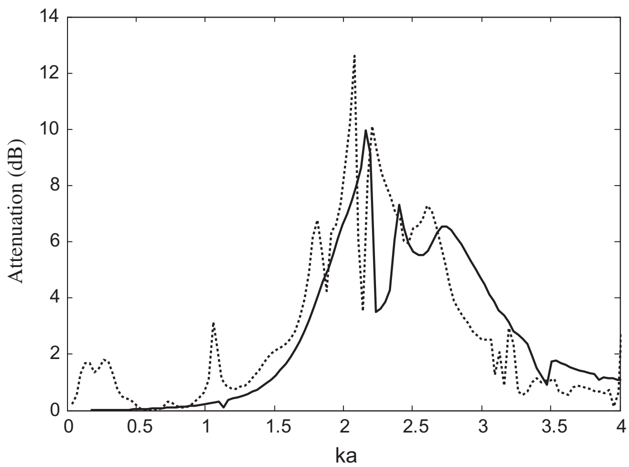

Fig. 16. The HQ-Liner analytical (bold) and measured (dotted) attenuation versus *ka* for a plane wave incident vector and $N_{HQ} = 1$.

Also, we note that, around the first HQ resonance frequency, a peak in the attenuation is experimentally observed unlike what was predicted by the model. It is likely due to uncertainties in the empirical liner impedance model whose dissipative effects mask the HQ effects at this frequency.

5. Conclusions

To study the efficiency of a serial association of a liner with a HQ section, an analytical computation of the HQ-Liner scattering matrix based on the overall algebraic product of the analytical scattering matrices of the HQ system and of the liner duct has been developed. This modelling was experimentally and numerically validated on a 1HQ-Liner configuration. The number of HQ tubes was shown to be the main parameter correlated with the modal conversion effect. Computation of the TL achieved for an incident plane wave vector from the scattering matrix of the HQ-Liner serial association shows that a very large benefit of this association is provided when the HQ configuration is chosen so that the plane wave reflection coefficient is increased around the liner resonance frequency. This optimal configuration results in a self state of stationary waves improving the liner efficiency.

In the future, a full model that uses a semi-analytical approach based on a boundary integral equation in the acoustic velocity, formulated over the saddle-shaped interface and solved by means, for instance, of a Galerkin approach, would still be computationally more efficient than FEM method and could improve the accuracy of the 3D formulation. The results obtained would benefit from experimental validation on a real turbofan configuration.

Acknowledgements

The authors would like to acknowledge the financial support of the CNRS and SNECMA, as well as insightful discussions with J. Julliard of SNECMA.

Appendix A

The liner is a Helmholtz resonator type material assumed to be locally reacting and made up of a perforated plate ($e = 0.001$ m thick, $\delta = 0.001$ m hole diameter and $\sigma = 5\%$ perforation rate), in contact with a $t = 0.02$ m thick honeycomb panel and backed by a rigid plate (Fig. 3) with a maximal efficiency at the non-dimensional frequency $ka = 2.18$.

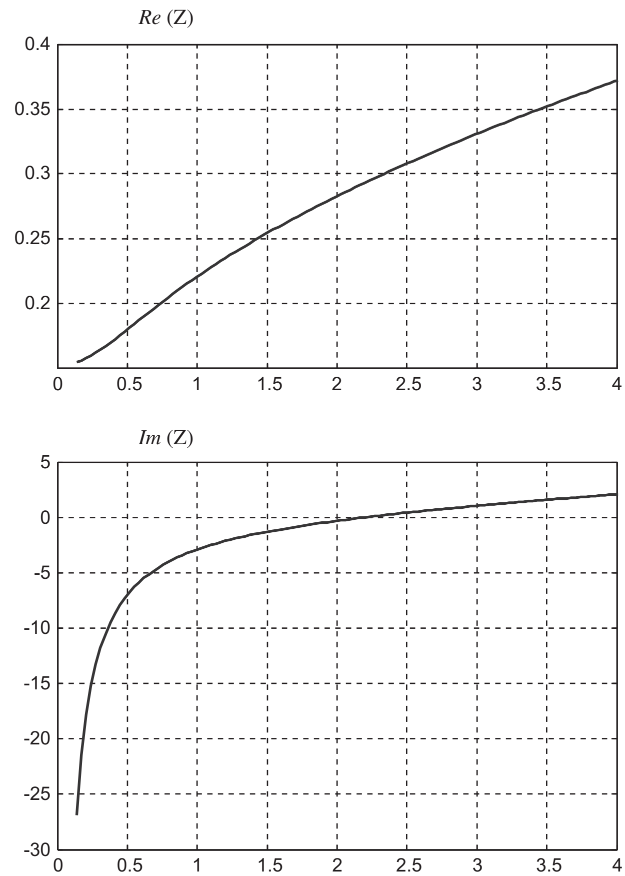

Fig. A.1. Real part and imaginary part of liner impedance *Z*.

The semi-empirical model of Elnady [15] was used to calculate the normalized acoustic impedance of the liner:

$$Z = R + iX \tag{A.1}$$

where

$$R = \frac{\sqrt{8\upsilon\omega}}{\sigma c}(1 + 1/d) \quad \text{at} \quad X = \frac{\omega(e + 0.8\sqrt{s})}{\sigma c} - \text{cotan}\left(\frac{\omega t}{c}\right) \tag{A.2}$$

where c is the celerity, υ the viscosity, s the hole section. The real and the imaginary part of normalized acoustic impedance are plotted versus *ka* in Fig. A.1.

Appendix B

Serial association of the scattering matrices.

The scattering matrices of two adjacent segments (see Fig. B.1) are defined by:

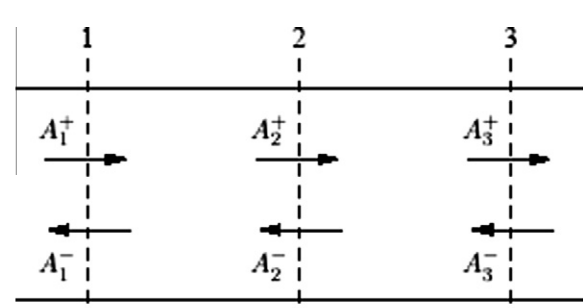

Fig. B.1. Schematic representation of a serial association.

$$\begin{pmatrix} A_2^+ \\ A_1^- \end{pmatrix} = S_{12}\begin{pmatrix} A_1^+ \\ A_2^- \end{pmatrix}, \quad \begin{pmatrix} A_3^+ \\ A_2^- \end{pmatrix} = S_{23}\begin{pmatrix} A_2^+ \\ A_3^- \end{pmatrix} \tag{B.1}$$

where the scattering matrices of the elements (1-2) and (2-3) are

$$S_{12} = \begin{pmatrix} T_{12} & R'_{12} \\ R_{12} & T'_{12} \end{pmatrix} \quad \text{et} \quad S_{23} = \begin{pmatrix} T_{23} & R'_{23} \\ R_{23} & T'_{23} \end{pmatrix} \tag{B.2}$$

A_1^- and A_3^+ are linked with A_1^+ and A_3^- by the global scattering matrix S_{13} defined as follows:

$$S_{13} = \begin{pmatrix} T_{23}\left(1-R'_{12}R_{23}\right)^{-1}T_{12} & R'_{23}+T_{23}\left(1-R'_{12}R_{23}\right)^{-1}R'_{12}T'_{23} \\ R_{12}+T'_{12}\left(1-R_{23}R'_{12}\right)^{-1}R_{23}T_{12} & T'_{12}\left(1-R_{23}R'_{12}\right)^{-1}T'_{23} \end{pmatrix} \tag{B.3}$$

Appendix C

To characterize the acoustic efficiency of the device, the acoustic power attenuation is used. It is defined as the ratio between the incoming and outgoing acoustic powers:

$$W_{\text{att}}(dB) = 10\log\left(\frac{W^{\text{in}}}{W^{\text{out}}}\right) \tag{C.1}$$

$W_{\text{att}}(dB)$ is deduced from the scattering matrix [20]. Indeed, these acoustic powers can be written in the following form:

$$W^{\text{in}} = \{\Pi^{\text{in}}\}_{2N}^{\text{H}} \cdot \{\Pi^{\text{in}}\}_{2N} \tag{C.2}$$

$$W^{\text{out}} = \{\Pi^{\text{out}}\}_{2N}^{\text{H}} \cdot \{\Pi^{\text{out}}\}_{2N} \tag{C.3}$$

where $\{\Pi^{\text{in}}\}_{2N}$ and $\{\Pi^{\text{out}}\}_{2N}$ are the modal intensities which can be written in term of respectively the incoming and outgoing modal pressures $\{P^{\text{in}}\}_{2N}$ and $\{P^{\text{out}}\}_{2N}$:

$$\begin{cases} \{\Pi^{\text{in}}\}_{2N} = [X]_{2N\times 2N}\cdot\{P^{\text{in}}\}_{2N}; \{\Pi^{\text{out}}\}_{2N} = [X]_{2N\times 2N}\cdot\{P^{\text{out}}\}_{2N} \\ \{\Pi^{\text{in}}\}_{2N}^{\text{T}} = \left\langle \Pi_{00}^{I+}(z_L),\ldots,\Gamma_{PQ}^{I+}(z_L),\Pi_{00}^{V-}(z_R),\ldots,\Pi_{PQ}^{V-}(z_R)\right\rangle \\ \{\Pi^{\text{out}}\}_{2N}^{\text{T}} = \left\langle \Pi_{00}^{I-}(z_L),\ldots,\Pi_{PQ}^{I-}(z_L),\Pi_{00}^{V+}(z_R),\ldots,\Pi_{PQ}^{V+}(z_R)\right\rangle \end{cases} \tag{C.4}$$

with

$$[X]_{2N\times 2N} = \begin{bmatrix} [diag(X_{mn})]_{N\times N} & [0]_{N\times N} \\ [0]_{N\times N} & [diag(X_{mn})]_{N\times N} \end{bmatrix}, X_{mn} = \sqrt{\frac{N_{mn}Sk_{mn}}{2\rho ck}} \tag{C.5}$$

and $\Pi_{mn}^{I\pm}(z_L) = X_{mn}P_{mn}^{I\pm}(z_L), \Pi_{mn}^{V\pm}(z_R) = X_{mn}P_{mn}^{V\pm}(z_R)$.

The scattering matrix relates the outgoing pressure waves to incoming pressure waves as follows:

$$\begin{aligned} \{\Pi^{out}\}_{2N} &= [S']_{2N\times 2N}\cdot\{\Pi^{in}\}_{2N} \\ &= [X]_{2N\times 2N}[S]_{2N\times 2N}[X]_{2N\times 2N}^{-1}\cdot\{\Pi^{in}\}_{2N} \end{aligned} \tag{C.6}$$

The matrix $[H]_{2N\times 2N}$ can be introduced as:

$$[H]_{2N\times 2N} = [S]_{2N\times 2N}^{H}\cdot[S]_{2N\times 2N}, \tag{C.7}$$

So that

$$[H]_{2N\times 2N} = [U]_{2N\times 2N}\cdot[\Lambda]_{2N\times 2N}\cdot[U]_{2N\times 2N}^{H} \tag{C.8}$$

where $[U]$ and $[\Lambda]$ are respectively the matrices of the eigenvectors and eigenvalues of $[H]$. After substituting (C.6) and (C.8) into (C.1) and (C.3), one obtains :

$$W_{\text{att}}(dB) = 10\log\left(\frac{\sum_{i=1}^{2N}|d_i|^2}{\sum_{i=1}^{2N}\lambda_i|d_i|^2}\right) \tag{C.9}$$

λ_i are the eigenvalues of the matrix $[H]$ and

$$\{d\}_{2N} = [U]_{2N\times 2N}^{\text{H}}\cdot\{\Pi^{in}\}_{2N} \tag{C.10}$$

Eq. (C.9) points out that the overall acoustic power attenuation depends upon the acoustic and geometrical properties of the test element and upon $\{P^{\text{in}}\}_{2N}$ the vector of the incoming modal pressures from the left and the right sides of the test duct element. For example, if $\{P^{\text{in}}\}_{2N} = \langle 1 \ \ 1 \ \ 1 \ \ 1 \ \ 1 \ \ 0 \ \ 0 \ \ 0 \ \ 0 \ \ 0\rangle^T$, the acoustic power attenuation is calculated assuming an acoustic incident pressure incoming only from the left side of the test duct element and distributed on the first five cut-on modes assumed to be in phase and equally excited with an amplitude equal to 1.

The transmission loss (TL) which takes into account both the reactive and dissipative properties of the test duct whereas the attenuation characterizes only the intrinsic dissipation of the test duct is defined by the ratio between the incident acoustic power W^{I+} and the transmitted acoustic power W^{V+}:

$$TL(dB) = 10\log\left(\frac{W^{I+}}{W^{V+}}\right) \tag{C.11}$$

References

[1] W Herschel JF. On the absorption of light by colored media, viewed in connection with the undulatory theory. Philoso Mag J Sci 1833;3:401–12.
[2] Burdisso R, Ng Wing F. Fan noise control using Herschel–Quincke resonators, NASA CR-2003-212097, 2003.
[3] Alonso Jose S, Burdisso R, Kan Hwa-Wan. Testing of adaptive HQ-Liner for aft noise. In: 14th AIAA/CEAS aeroacoustics conference, 2008.
[4] de la Riva, DH, Burdisso R, Ng W. Aft fan noise control using Herschel/Quincke-liner systems. In: 14th AIAA/CEAS aeroacoustics conference, 2008.
[5] Fuller CR, Bies DA. A reactive acoustic attenuator. J Sound Vib 1978;56(1):45–59.
[6] Depollier C, Kergomard J, Lesueur JC. Propagation of low frequency acoustic waves in periodic 2-D lattices of tubes. J Sound Vib 1990;142(1):153–70.
[7] Selamet A, Dickey NS, Novak JM. The Herschel–Quincke tube: a theoretical, computational, and experimental investigation. J Acoust Soc Am 1994;96(5):3177–95.
[8] Selamet A, Easwaran V. Modified Herchel–Quincke tube: attenuation and resonance for N-duct configuration. J Acoust Soc Am 1997;102(1):164–9.
[9] Torregrosa AJ, Broatch A, Payri R. A study of the influence of mean flow on the acoustic performance of Herschel–Quincke tubes. J Acoust Soc Am 2000;107(4):874–1879.
[10] Karlsson M, Glav R, Abom M. The Herschel–Quincke tube: the attenuation conditions and their sensitivity to mean flow. J Acoust Soc Am 2008;124(2):723–32.
[11] Poirer B, Ville JM, Maury C, Kateb D. Bicylindrical model of Herschel–Quincke tube duct system: theory and comparison with experiment and finite element method. J Acoust Soc Am 2009;126(3):1151–62.
[12] Bi, Pagneux, Aurégan Y. Modelling of sound propagation in a non-uniform lined duct using a multi modal propagation method. J Sound Vib 2006;289(4–5):1091–111.
[13] Sitel A, M Ville J, Foucart F. Multiload procedure to measure the acoustic scattering matrix of a duct discontinuity for higher order mode propagation conditions. J Acoust Soc Am 2006;120(5):2478–90.
[14] Hallez RF, P Smith J, A Burdisso R. Control of higher-order modes in ducts using arrays of Herschel–Quincke waveguides. ASME Control Vib Noise 2000.
[15] Elnady T. On semi-empirical liner impedance modeling with grazing flow. In: 9th AIAA/CEAS aeroacoustic conference, Hilton Head (SC, USA): May 12–14, 2003. p. 3304.
[16] Becache E, Bonnet A-S, Legendre Perfectly G. Matched layers for the convected Helmoltz equation. SIAM J Numer Anal 2004;42(1):409–33.
[17] Akoum M, M Ville J. Measurement of reflection matrix of a discontinuity in a duct. J Acoust Soc Am 1998;103(5):2463–8.
[18] Auger JM, Ville JM. Measurement of liner impedance based on the determination of duct eigenvalues by Fourier–Lommel's transform. J Acoust Soc Am 1990;88(1):19–22.
[19] Taktak M. Mesure de la matrice de diffusion d'un tronçon traité cylindrique recouvert par un matériau: applications à la mesure de son efficacité et à la détermination de son impédance homogénéisée. Thèse de Doctorat, Université de Technologie de Compiègne; 2008.
[20] Aurégan Y, Starobinski R. Determination of Acoustical energy dissipation/production potentiality from the acoustical transfer functions of a multiport. Acust Acta Acust 1999;85:788–92.